Frequency Response Method for Investigation of Kinetic Details of a Heterogeneous Catalyzed Reaction of Gases

Yusuke Yasuda,* Hitoshi Mizusawa, and Takeshi Kamimura

Faculty of Science, Toyama University, Toyama 930-8555, Japan

Received: November 20, 2001; In Final Form: April 10, 2002

A novel frequency response (FR) method is proposed: (i) Partial pressure(s) of reactant(s) in a steady-flow reactor is perturbed sinusoidally by varying gas space of the reactor with a definite angular frequency ω; (ii) amplitude and phase shift of every partial-pressure variation of both reactant(s) and product(s) is measured over a wide range of ω; (iii) on the other hand, characteristic functions of ω to explain "reaction-rate spectra" obtained from the data in (ii) are deduced analytically on the basis of a reaction mechanism; and (iv) complex rate coefficients, $(k + i\omega l)$, involved in the functions are determined by numerical simulation to the spectra. The FR method is applied to CO oxidation over Ru/Al_2O_3 at ca. 10^2 Pa and 623 K in order to confirm its efficiency: (i) As many as thirteen rate coefficients at five elementary steps were determined; (ii) chemical potentials of surface-intermediates, CO(a), O_2(a), and O(a), were derived from l's; and (iii) free-energy dissipations via the three intermediates were deduced from chemical potential changes at five elementary steps. It is concluded that the reaction sequence of carbon monoxide, $CO(g) \rightarrow CO(a) \rightarrow CO_2(g)$, could occur spontaneously but the other sequence of oxygen, $^1/_2O_2(g) \rightarrow {}^1/_2O_2(a) \rightarrow O(a) \rightarrow CO_2(g)$, would be against the reaction, although they are coupled.

1. Introduction

Quantitative description of a heterogeneous catalyzed reaction *rate* seems indispensable to develop chemical kinetics of catalysis. However, it is usually difficult because of multisteps contained in a reaction mechanism.

The formation of CO_2 through catalytic oxidation of carbon monoxide is the best understood catalytic reaction, because the reaction mechanism and kinetics are relatively simple compared with other catalytic processes.[1,2] Even for the simple-seeming reaction, however, spatio-temporal patterns and also standing waves of surface species have been observed on Pt(110),[3,4] which means that a traditional rate expression in terms of (uniform) concentrations is invalid. The standing wave patterns have been reproduced well by numerical simulations based on an extended reaction−diffusion model containing surface diffusion; the simultaneous differential equations of the model involve more than sixteen adjustable parameters despite the simple reaction.[4] Consequently, it seems almost hopeless to describe quantitatively kinetic details of elementary reactions occurring on practical catalysts.

A variety of transient methods have been proposed to investigate a heterogeneous catalyzed reaction.[5,6] The composition of a stream in steady flow to an open reactor is perturbed (step function, pulse, sine or square wave, etc.) and the response of the system to the signal is measured. In a frequency response (FR) method the concentration of reactant(s) in a flow reactor is periodically perturbed by sinusoidal input[7] or sinusoidal variation of the gas space.[8,9] The advantages of the latter are as follows: (i) Since the perturbation may be very small, any rate equations can be linearized by Taylor series expansion to the first order; (ii) since the perturbation is harmonic, simultaneous differential equations for elementary reactions can be analytically solved; and (iii) since the frequency ω can be easily scanned over a wide range, all adjustable parameters involved in characteristic functions of ω can be determined by numerical simulation over the whole range.[10,11]

In this work the latter FR method is applied to a CO oxidation reaction over Ru/Al_2O_3 powders in order to confirm availability of the present method.

2. Experimental Section

The FR apparatus is schematically shown in Figure 1. A gas mixture of CO, O_2, and Ar was admitted to the flow reactor with a constant rate of supply, in which the partial pressure of each component was ca. 10 Pa; 0.5 wt % Ru/Al_2O_3 (177 m^2/g, 1.8 g; reference catalyst of JRC-A4-0.5Ru, The Catalysis Society of Japan) was kept at 623 K; Ar was added as a reference standard because neither adsorption−desorption nor reaction occurred.

The gas space of the flow reactor was varied sinusoidally by stainless steel bellows. The variation was expressed well (using complex notation) by

$$V(t) = V + \Delta V(t); \quad \Delta V(t)/V = -\upsilon \exp(i\omega t) \qquad (1)$$

where V denotes the mean volume (ca. 1 dm^3), υ is the relative amplitude (ca. 4%), and ω is the angular frequency which was scanned over a range between 80 and 2.5 rad/min corresponding to 0.2 and 0.007 Hz, respectively.

The partial pressure variation of a component W, $P_W(t)$, was expressed in general by

$$P_W(t) = P_W + \Delta P_W(t); \quad \Delta P_W(t)/P_W = p_W^* \exp(i\omega t); \quad p_W^* \equiv p_W \exp(i\phi_W) \qquad (2)$$

where P_W denotes the partial pressure at a steady state, p_W is the relative amplitude, and ϕ_W is the phase difference between the volume and pressure variations.

* Author to whom all correspondence should be addressed. E-mail: yasuda@sci.toyama-u.ac.jp.

10.1021/jp014295u CCC: $22.00
Published on Web 06/07/2002

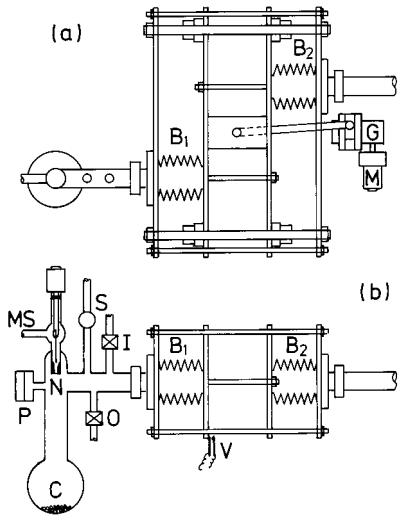

Figure 1. Schematic diagram of the FR apparatus. (a) Top- and (b) side-views. B_1 and B_2: stainless-steal bellows (15 cm diameter tme 20 cm length); B_2 is valid to compensate atmospheric pressure for B_1; C: catalysts; G: gear box to generate sinusoidal oscillation; I: inlet variable-leak valve (Granville-Philip, Type 24); M: variable-speed motor; MS: mass spectrometer (Balzers Quadstar 422); N: needle valve; O: outlet variable-leak valve (Granville-Philip, Type 24); P: pressure gauge (Baratron, Type 223BD); S: stopcock; V: on−off switch to detect the position at volume maximum.

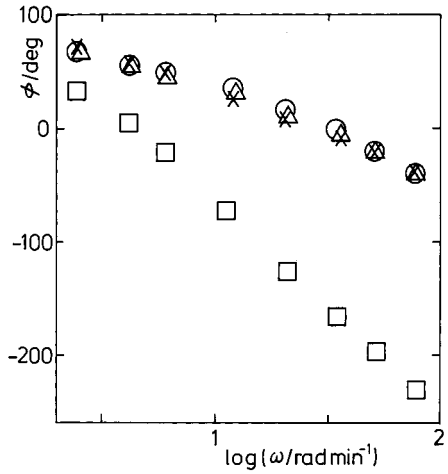

Figure 2. Phase differences between each partial-pressure and volume variations, ϕ, versus angular frequency ω at 623 K; the partial pressures of CO(△), O_2(○), CO_2(□), and Ar(×) at the steady state were 0.29, 0.15, 0.10, and 0.20 Torr (1 Torr = 133.32 Pa), respectively.

The pressure variation of each component was monitored by a mass spectrometer and p_W and ϕ_W were observed at a definite ω which was scanned over a wide range. The scan of ω for each component was carried out successively over that range.

The sensitivity of the mass spectrometer calibrated for every component was nearly proportional to its molecular weight.

3. Results

The actual data on ϕ_W and p_W are plotted versus ω in Figures 2 and 3, respectively. To remove apparent change due to the apparatus, the in-phase and out-of-phase components, $f_{cW}^{(exp)}$ and $f_{sW}^{(exp)}$, respectively, were determined by the ratio (p_W/p_0) and the difference $(\phi_W - \phi_0)$:

$$(p_W/p_0)\cos(\phi_W - \phi_0) - 1 \equiv f_{cW}^{(exp)}(\omega) \quad (3)$$

$$(p_W/p_0)\sin(\phi_W - \phi_0) \equiv f_{sW}^{(exp)}(\omega) \quad (4)$$

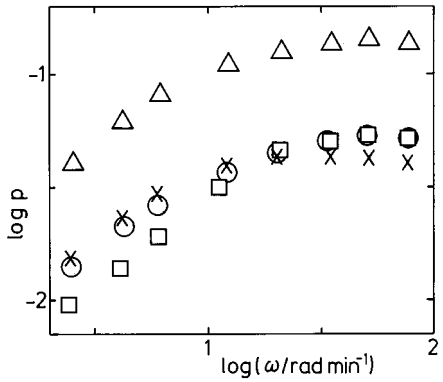

Figure 3. Relative amplitude of each partial-pressure variation, p, versus angular frequency ω. Notation is that of Figure 2.

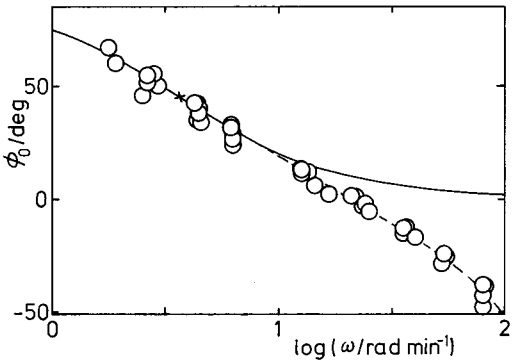

Figure 4. Results of ϕ_0 (i.e., Ar) obtained in separate runs are plotted together. The solid line represents a theoretical curve given by eq 32, of which adjustable parameter σ was 3.67 min^{-1}.

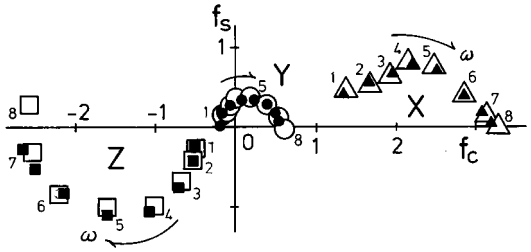

Figure 5. Rectangular plots of the in-phase and out-of-phase components, (f_{cW}, f_{sW}). Open symbols represent the experimental results, $(f_{cW}^{(exp)}, f_{sW}^{(exp)})$, given by eqs 3 and 4; solid symbols represent the calculated ones, $(f_{cW}^{(calc)}, f_{sW}^{(calc)})$ which were evaluated by eqs 26−28 with thirteen adjustable parameters given in Table 1. The number indicates the value of $\log(\omega_j/\text{rad min}^{-1})$: **1**(= 0.45), **2**(= 0.65), **3**(= 0.85), **4**(= 1.05), **5**(= 1.25), **6**(= 1.45), **7**(= 1.65), **8**(= 1.85).

where the subscript 0 means an inert gas (i.e., Ar in this work).

The results of ϕ_0 observed in separate runs are plotted together in Figure 4 to demonstrate the accuracy of the phase shift measurements.

The data of ϕ_W and p_W shown in Figures 2 and 3 were interpolated using polynomials in log ω to eight ω_j's given by $\omega_1 = 10^{0.45}$, $\omega_2 = 10^{0.65}$, $\omega_3 = 10^{0.85}$, $\omega_4 = 10^{1.05}$, $\omega_5 = 10^{1.25}$, $\omega_6 = 10^{1.45}$, $\omega_7 = 10^{1.65}$, and $\omega_8 = 10^{1.85}$; the in-phase and out-of-phase components of eqs 3 and 4 at every ω_j are plotted using rectangular coordinates in Figure 5. It seems of interest that those of both reactants of X(CO) and Y(O_2), and those of the product of Z(CO_2) are on the opposite side of the origin. Since the origin corresponds to the results of Ar, the deviation from the origin can be ascribed to the variation in each reaction *rate*.[9]

In blank experiments carried out with single component of either CO or O_2 (together with Ar for reference), both

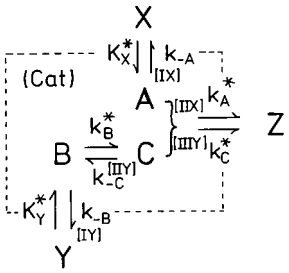

Figure 6. An extended reaction mechanism. (X) represents CO(gas); (Y), (1/2)O_2(gas); (Z), CO_2(gas); (A), CO(ads); (B), (1/2)O_2(ads); (C), O(ads). Rate coefficient at each elementary reaction is indicated beside each arrow; K_X*, for example, means $K_X + i\omega L_X$. IX and IIX indicate the two steps concerning X; IY, IIY, and IIIY indicate the three steps concerning Y.

components in eqs 3 and 4 were negligibly small so that contributions of adsorption−desorption concerning CO and O_2 can be neglected.

4. Data Analysis

4.1. Expressions for $\Delta A(t)$, $\Delta B(t)$, and $\Delta C(t)$. The reaction mechanism of carbon monoxide oxidation over platinum group metals that is widely accepted[1,2] is shown in Figure 6, where every molecular species is represented by a single letter for simplicity. Although the first step of O_2(gas) ⇆ O_2(ads) concerning oxygen, IY, has usually been ignored,[1,2] it is included in this extended mechanism.

Since the perturbation to the system at a steady state is usually very small, any rate equation of an elementary reaction can be linearized by Taylor series expansion as follows.[10]

The appearance rate of surface-species CO(a), dA/dt, for example, may be described by

$$\mathrm{d}A(t)/\mathrm{d}t = K_X^*\Delta P_X(t) - k_{-A}\Delta A(t) - k_A^*\Delta A(t) - k_C^*\Delta C(t) \quad (5)$$

where $\Delta P_X(t)$, $\Delta A(t)$, and $\Delta C(t)$ denote each variation induced by the volume change, ΔV; the last term on the right-hand side arises from $\Delta P_Y(t)$; the expansion coefficients, K_X*, k_{-A}, k_A*, and k_C* (which will be named rate coefficients) are indicated beside each arrow of the elementary reaction in Figure 6. The superscript * means that the rate coefficient K_X*, for example, is complex defined by $K_X + i\omega L_X$. Basic assumption in the present method is that "every rate coefficient for the *forward* reaction is expressed by a complex rate coefficient".[10,11] It agrees with traditional one in an extreme case of $l = 0$. It is worth noting that l's have not been observed by a traditional steady-state method because they vanish when $\omega = 0$.

The time derivative d/dt can be replaced by $i\omega$ because of the harmonic oscillation so that eq 5 can be rewritten as

$$(k_{-A} + k_A^* + i\omega)\Delta A(t) + k_C^*\Delta C(t) = K_X^*\Delta P_X(t) \quad (6)$$

In a similar way to dB(t)/dt and dC(t)/dt, we have

$$(k_{-B} + k_B^* + i\omega)\Delta B(t) - k_{-C}\Delta C(t) = K_Y^*\Delta P_Y(t) \quad (7)$$

and

$$k_A^*\Delta A(t) - k_B^*\Delta B(t) + (k_{-C} + k_C^* + i\omega)\Delta C(t) = 0 \quad (8)$$

The simultaneous equations of eqs 6−8 can be easily solved and we have

$$\Delta A(t) = [\{\Theta + k_A^*(k_{-B} + k_B^* + i\omega)k_C^*\}/\{(k_{-A} + k_A^* + i\omega)\Theta\}]K_X^*\Delta P_X(t) - (k_B^*k_C^*/\Theta)K_Y^*\Delta P_Y(t) \quad (9)$$

$$\Delta B(t) = -(k_A^*k_{-C}/\Theta)K_X^*\Delta P_X(t) + [\{\Theta + (k_{-A} + k_A^* + i\omega)k_B^*k_{-C}\}/\{(k_{-B} + k_B^* + i\omega)\Theta\}]K_Y^*\Delta P_Y(t) \quad (10)$$

$$\Delta C(t) = \{(k_{-A} + k_A^* + i\omega)(k_{-B} + k_B^* + i\omega)/\Theta\} \times [-\{k_A^*/(k_{-A} + k_A^* + i\omega)\}K_X^*\Delta P_X(t) + \{k_B^*/(k_{-B} + k_B^* + i\omega)\}K_Y^*\Delta P_Y(t)] \quad (11)$$

where the abbreviation

$$\Theta \equiv (k_{-A} + k_A^* + i\omega)(k_{-B} + k_B^* + i\omega)(k_{-C} + k_C^* + i\omega) - k_A^*(k_{-B} + k_B^* + i\omega)k_C^* - (k_{-A} + k_A^* + i\omega)k_B^*k_{-C} \quad (12)$$

is introduced.

4.2. Expressions for $f_{cX}^{(calc)}(\omega)$ and $f_{sX}^{(calc)}(\omega)$. If spatial uniformity of each component through the reactor is fulfilled (this is the fundamental assumption in the present method), the disappearance rate of CO molecules in gas phase, dX(t)/dt, may be described by

$$\mathrm{d}X(t)/\mathrm{d}t = J_X - K_X^*\Delta P_X(t) + k_{-A}\Delta A(t) - \sigma'\{P_X + \Delta P_X(t)\} \quad (13)$$

where J_X denotes the steady feed of gaseous CO and the flow of outlet is given by $\sigma' P_X(t)$. On the other hand, since every component in the gas phase may be regarded as an ideal gas, $X(t)$ can be expressed by

$$X(t) = P_X(t)V(t)/(RT_0) \quad (14)$$

Substituting eqs 1 and 2 into eq 14, we have

$$X(t) = \{P_X V/(RT_0)\}\{1 + (p_X^* - \upsilon)\exp(i\omega t)\} \quad (15)$$

The second-order term of $p_X^*\upsilon \exp(2i\omega t)$ can be neglected in this work.

Combining eqs 13 and 15 and substituting eq 9 for ΔA, we have after some rearrangements

$$(\sigma + i\omega)p_X^* - i\omega\upsilon = (\alpha - 1)k_X^*p_X^* - (k_{-A}k_B^*k_C^*/\Theta)(P_Y/P_X)k_Y^*p_Y^* \quad (16)$$

where the short notation

$$k_X^* \equiv (RT_0/V)K_X^*,\ k_Y^* \equiv (RT_0/V)K_Y^*,\ \sigma \equiv (RT_0/V)\sigma' \quad (17)$$

and the abbreviation

$$\alpha \equiv k_{-A}\{\Theta + k_A^*(k_{-B} + k_B^* + i\omega)k_C^*\}/\{\Theta(k_{-A} + k_A^* + i\omega)\} \quad (18)$$

is introduced.

If eq 16 is applied to Ar, every rate coefficient vanishes so that we have

$$(\sigma + i\omega)p_0^* - i\omega\upsilon = 0 \quad (19)$$

TABLE 1: Every Rate Coefficient Evaluated by Numerical Simulation (min^{-1} units for *k*'s)

k_X[a]	l_X[a]	k_{-A}	k_A	l_A	k_Y[a]	l_Y[a]	k_{-B}	k_B	l_B	k_{-C}	k_C	l_C
−1.73	−0.75	−0.39	0.065	0.096	1.61	−0.35	2.4	0.68	−0.28	0.80	0.70	−0.68

[a] $k_X \equiv (RT_0/V)K_X$, $l_X \equiv (RT_0/V)L_X$, $k_Y \equiv (RT_0/V)K_Y$, $l_Y \equiv (RT_0/V)L_Y$.

Subtracting eq 19 from eq 16, we have

$$(\sigma + i\omega)(p_X^* - p_0^*) = (\alpha - 1)k_X^* p_X^* - (k_{-A}k_B^* k_C^*/\Theta)(P_Y/P_X)k_Y^* p_Y^* \quad (20)$$

Dividing both sides of eq 20 by p_0^*, we have the final result:

$$(p_X^*/p_0^*) - 1 = \{1/(\sigma + i\omega)\}\{(\alpha - 1)k_X^*(p_X^*/p_0^*) - (P_Y/P_X)(k_{-A}k_B^* k_C^*/\Theta)k_Y^*(p_Y^*/p_0^*)\} \quad (21)$$

Since the ratio (p_X^*/p_0^*) can be rewritten as $(p_X/p_0)\exp\{i(\phi_X - \phi_0)\}$, the real and imaginary parts on both sides lead to the theoretical expressions for $f_{cX}^{(exp)}(\omega_j)$ and $f_{cX}^{(exp)}(\omega_j)$; they will be represented by $f_{cX}^{(calc)}(\omega_j)$ and $f_{sX}^{(calc)}(\omega_j)$.

4.3. Expressions for $f_{cW}^{(calc)}(\omega)$ and $f_{sW}^{(calc)}(\omega)$. According to similar procedure to d$Y(t)$/dt, we have

$$(p_Y^*/p_0^*) - 1 = \{1/(\sigma + i\omega)\}\{-(P_X/P_Y)((k_A^* k_{-B}k_{-C}/\Theta)k_X^*(p_X^*/p_0^*) + (\beta - 1)k_Y^*(p_Y^*/p_0^*)\} \quad (22)$$

where β is defined as

$$\beta \equiv k_{-B}\{\Theta + (k_{-A} + k_A^* + i\omega)k_B^* k_{-C}\}/\{\Theta(k_{-B} + k_B^* + i\omega)\} \quad (23)$$

Further, according to similar procedure to d$Z(t)$/dt, we have

$$(p_Z^*/p_0^*) - 1 = \{1/(\sigma + i\omega)\}[(P_X/P_Z)\gamma k_X^*(p_X^*/p_0^*) + (P_Y/P_Z)\{(k_{-A} + i\omega)k_B^* k_C^*/\Theta\}k_Y^*(p_Y^*/p_0^*)] \quad (24)$$

where γ is defined as

$$\gamma \equiv k_A^*\{\Theta + k_A^*(k_{-B} + k_B^* + i\omega)k_C^* - (k_{-A} + k_A^* + i\omega)(k_{-B} + k_B^* + i\omega)k_C^*\}/\{\Theta(k_{-A} + k_A^* + i\omega)\} \quad (25)$$

These final results are rewritten as follows:

$$f_{cX}^{(calc)} + if_{sX}^{(calc)} = \{1/(\sigma + i\omega)\}[J_{XX}^*(\omega)(p_X^*/p_0^*) + J_{XY}^*(\omega)(P_Y/P_X)(p_Y^*/p_0^*)] \quad (26)$$

$$f_{cY}^{(calc)} + if_{sY}^{(calc)} = \{1/(\sigma + i\omega)\}[J_{YX}^*(\omega)(P_X/P_Y)(p_X^*/p_0^*) + J_{YY}^*(\omega)(p_Y^*/p_0^*)] \quad (27)$$

$$f_{cZ}^{(calc)} + if_{sZ}^{(calc)} = \{1/(\sigma + i\omega)\}[J_{ZX}^*(\omega)(P_X/P_Z)(p_X^*/p_0^*) + J_{ZY}^*(\omega)(P_Y/P_Z)(p_Y^*/p_0^*)] \quad (28)$$

where X, Y, and Z denote CO, O_2, and CO_2, respectively; the coefficient J^*'s are given explicitly in terms of rate coefficients by

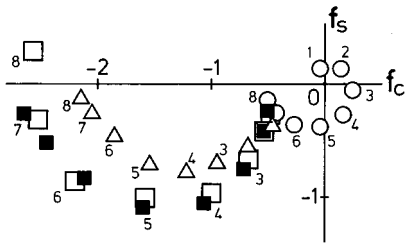

Figure 7. Contributions of $\Delta P_X(t)$ and $\Delta P_Y(t)$ to the appearance rate of Z calculated: (△) indicates contribution of the first term due to ΔP_X given in eq 28; (○), contribution of the second term due to ΔP_Y given in eq 28; (■), the sum of these two terms; (□) is the experimental ones that are the same as those shown in Figure 5.

$$J_{XX}^*(\omega) = (\alpha - 1)k_X^* \text{ and } J_{XY}^*(\omega) = -(k_{-A}k_B^* k_C^*/\Theta)k_Y^* \quad (29)$$

$$J_{YX}^*(\omega) = -(k_A^* k_{-B}k_{-C}/\Theta)k_X^* \text{ and } J_{YY}^*(\omega) = (\beta - 1)k_Y^* \quad (30)$$

$$J_{ZX}^*(\omega) = \gamma k_X^* \text{ and } J_{ZY}^*(\omega) = \{(k_{-A} + i\omega)k_B^* k_C^*/\Theta\}k_Y^* \quad (31)$$

4.4. Evaluation of σ. The value of σ can be determined as follows: Real parts of eq 19 lead to

$$\phi_0(\omega) = \tan^{-1}(\sigma/\omega) \quad (32)$$

The calculated result of eq 32 is shown by the solid curve in Figure 4 where σ was chosen as 3.67 min^{-1} in consideration of $\phi_0(\sigma) = \tan^{-1}(1) = 45°$. The deviation of actual data from the solid curve may be attributed to delay due to bottleneck of the needle valve at the entrance of the mass spectrometer (see Figure 1); evidently, eq 13 is valid irrespective of the delay.

4.5. Evaluation of Rate Coefficients. The values of $f_{cW}^{(calc)}$ and $f_{sW}^{(calc)}$ in eqs 26−28 were determined semiempirically: (p_W^*/p_0^*) were replaced by experimental data and the adjustable parameters were determined on a trial and error basis by a personal computer to reproduce $(f_{cW}^{(exp)}, f_{sW}^{(exp)})$ as close as possible in Figure 5. Practically, the thirteen parameters were divided into five parameters concerned with ΔP_X and eight parameters concerned with ΔP_Y, although they are coupled; the five were optimized for every data of X, Y, and Z, $(f_{cw}^{(exp)}, f_{sw}^{(exp)})$ with appropriate eight parameters and then the other eight were optimized also for every data of X, Y, and Z, $(f_{cw}^{(exp)}, f_{sw}^{(exp)})$; the optimization was alternately repeated. The calculated results are compared with experimental ones in Figure 5, of which parameters are given in Table 1.

The contributions of the first and second terms on the right-hand side of eqs 26−28 due to ΔP_X and ΔP_Y can be determined separately: That of ΔP_Y (not ΔP_X) to the disappearance rate of X, dX/dt, in eq 26 was less than 0.06; that of ΔP_X for the disappearance rate of Y, dY/dt, in eq 27 was less than 0.07. Both contributions to appearance rate of Z, dZ/dt, are shown individually in Figure 7; that of ΔP_X was superior to that of ΔP_Y.

5. Discussion

5.1. Reaction-Rate Spectroscopy. Since every rate coefficient is involved in all J^*'s in eqs 29−31, all elementary

reactions are more or less coupled with each other, which denies the concept of a rate-determining step usually adopted in the formulation of catalytic kinetics.[12] It should be emphasized that the variable ω played an essential role to evaluate as many as thirteen rate coefficients in this work so that the FR method may be named "reaction-rate spectroscopy" similar to "relaxation spectroscopy" suggested by Eigen.[5]

Reliability of the rate coefficients in Table 1 evidently depends on accuracy of the FR data; the accuracy of phase lag was within ca. 5 degrees (see Figure 4) and that of amplitude was within ca. 20%. However, since the scan of ω for each component was performed in series, the results of ratio, p_W/p_0, would be more accurate than the single values of p_0. The accuracy of the computer simulation depends also on the range of ω scanned. The range covered in this work seems almost satisfactory, because the measurements at ω lower than ω_1 and also at ω higher than ω_8 would not be important so much for the simulation in Figure 5.

5.2. Results of *k*'s. K_X^* (and therefore both k_X and l_X) ought to depend on the amounts of catalysts. On the other hand, because dA/dt and also ΔA and ΔC depend on the amount of catalysts, their coefficients, k_{-A}, k_A^*, and k_C^*, should be independent of the amounts of catalysts.

Units of all k's are min^{-1} so that every elementary reaction rate can be compared with each other;[13] for example, $k_{-B}/(k_{-B} + k_B)$ gives the probability of the reverse reaction concerned with B-species; $1/(k_{-B} + k_B)$ gives a mean residence time of B-species provided that the forward and reverse rates are proportional to B. On the other hand, the variations of forward and reverse reaction-rates at IIY, B $\rightarrow$ C and B $\leftarrow$ C, for example, are given by $k_B\Delta B$ and $k_{-C}\Delta C$, respectively. However, since ΔB and ΔC given by eqs 10 and 11 depend on ω, their comparison would not be effective.

The negative value of k_X must not be discarded but may be explained by negative power of P_X in a rate expression such as $r = k'P_Y/P_X$ that is often observed at higher coverage of CO and higher reaction temperature on platinum group metals.[2]

5.3. Results of *l*'s. The elementary reaction rate R at both IIX and IIIY,

$$\mathrm{CO(ads)} + \mathrm{O(ads)} \rightarrow \mathrm{CO_2(gas)} \tag{33}$$

is oscillated by ΔV and the variation is represented by

$$\Delta R(t) = (k_A + i\omega l_A)\Delta A(t) \tag{34}$$

and also by

$$\Delta R(t) = (k_C + i\omega l_C)\Delta C(t) \tag{35}$$

Since $\Delta A(t)$, for example, varies sinusoidally, eq 34 can be rewritten as

$$\Delta R(t) = k_A\Delta A + l_A(\mathrm{d}A(t)/\mathrm{d}t) \tag{36}$$

According to Fick's second law of diffusion, the second term in eq 36 can be related to inhomogeneous A-species by $\partial A/\partial t = D(\partial^2 A/\partial x^2)$. Therefore, spatio-temporal patterns[3] could be characterized by l's.

Angular distribution of CO_2 formed on Pt group metals has been studied.[2] Recently, translational energy of desorbing product CO_2 in steady-state CO oxidation on Pd(110) was observed in the CO pressure range of 1×10^{-6} to 1×10^{-4} Torr (1 Torr = 133.32 Pa) at constant O_2 pressure; the CO_2 desorption was always collimated along the surface-normal direction.[14] It is known that adsorbed CO moves quickly on the surface and CO_2 formation is likely to take place on oxygen adsorption sites. Although the pressure range is very different from that in this work (named pressure gap problem), the different behavior of CO(g) and O_2(g) seems favorable to the opposite signs in l_A and l_C.

Contrary to previous results that both l_X and l_Y were zero in a catalytic hydrogenation reaction of propene,[10,11] l_X and l_Y in this work were not zero (see Table 1). The different results might be attributed to the different amount of catalysts, because a quite different reactor composed of proton-conducting membrane was used in the hydrogenation reaction.

5.4. Interpretation of *l*'s. *5.4.1. Two-Step Model of X $\leftrightarrows$ A $\rightarrow$ Z.* On the basis of a three-step model, the coefficient l's have been correlated with free-energy dissipations via surface intermediates.[11] According to a similar procedure, the free-energy dissipation via A-species, w_A, may be described by

$$Aw_A = \mu_{IX}(S_{IX} - S_{-IX}) - \mu_{IIX}R \tag{37}$$

where A denotes the amount of A-species; S_{IX} and S_{-IX} denote the forward and reverse rates, respectively, at IX; the free energy drops are indicated by $\mu_{IX}(\equiv \mu_X - \mu_A)$ and $\mu_{IIX}(\equiv \mu_A - \mu_Z)$, where μ_X, μ_A, and μ_Z denote the chemical potentials of X-, A-, and Z-species, respectively.

The variation of w_A induced by ΔV can be given by[11]

$$\Delta w_A = \{\mu_{IX} + l_A(\mu_{IX} - \mu_{IIX})\}(\mathrm{d}A/\mathrm{d}t)/A \tag{38}$$

Considering the requirement of $\Delta w_A = 0$ [15] and the definition of $\mu_{IX} + \mu_{IIX} = \mu_X - \mu_Z(\equiv \mu_{XZ})$, we have

$$\mu_{IX} = \{l_A/(1 + 2l_A)\}\mu_{XZ} \tag{39}$$

$$\mu_{IIX} = \{(1 + l_A)/(1 + 2l_A)\}\mu_{XZ} \tag{40}$$

Substituting eqs 39 and 40 into eq 37, we have at a steady state

$$Aw_A = -\{1/(1 + 2l_A)\}\mu_{XZ}R \tag{41}$$

where $S_{IX} - S_{-IX}$ is replaced by R.

Because l_A corresponds to the Taylor series expansion coefficient, $(\partial R/\partial(\mathrm{d}A/\mathrm{d}t))$,[10,11] the value should be less than unity:

$$|l_A| < 1 \tag{42}$$

This condition is satisfied with l_A in Table 1.

5.4.2. Three-Step Model of Y $\leftrightarrows$ B $\leftrightarrows$ C $\rightarrow$ Z. The other reaction sequence of Y $\leftrightarrows$ B $\leftrightarrows$ C $\rightarrow$ Z in Figure 6 is composed of three steps so that the results derived previously[11] can be applied, which may be rewritten in this case as follows:

$$\mu_{IY} = (l_B l_C/L)\mu_{YZ} \tag{43}$$

$$\mu_{IIY} = \{(1 + l_B)l_C/L\}\mu_{YZ} \tag{44}$$

$$\mu_{IIIY} = \{(1 + l_B)(1 + l_C)/L\}\mu_{YZ} \tag{45}$$

where the short notation is introduced:

$$L \equiv 1 + l_B + 2l_C + 3l_B l_C \tag{46}$$

Considering eqs 43−45, we may have expressions for free-energy dissipations via B- and C-species, w_B and w_C, respectively:

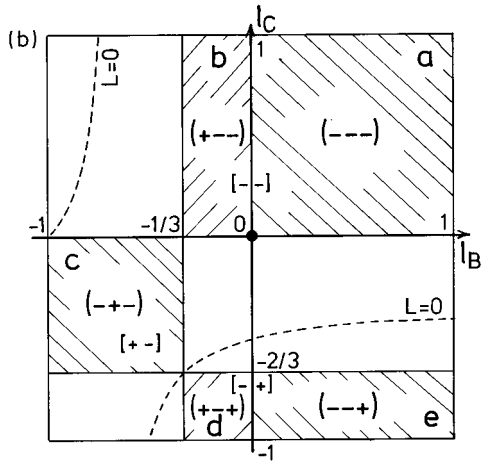

Figure 8. Allowed area for l_B and l_C given by eq 50 is divided into several zones with different sets of signs for ($-\mu_{IY}$, $-\mu_{IIY}$, $-\mu_{IIIY}$) and [Bw_B, Cw_C].

TABLE 2: Chemical Potential Drops in the Reaction Sequence of X → A → Z and Free-Energy Dissipation via A-Species (μ_{XZ} units)

$-\mu_{IX}$	$-\mu_{IIX}$	Aw_A/R
−0.08	−0.92	−0.84

TABLE 3: Chemical Potential Drops in the Reaction Sequence of Y → B → C → Z and Free-Energy Dissipations via B- and C-species (μ_{YZ} units)

$-\mu_{IY}$	$-\mu_{IIY}$	$-\mu_{IIIY}$	Bw_B/R	Cw_C/R	$(Bw_B + Cw_C)/R$
2.7	−6.9	3.2	−9.6	10.1	0.51

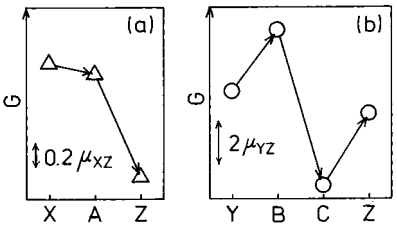

Figure 9. Chemical potential changes of each component in the course of sequential reactions, of which values are given in Tables 2 and 3. Notation is that of Figure 6.

$$Bw_B = -(l_C/L)\mu_{YZ}R \tag{47}$$

$$Cw_C = -\{(1 + l_B)/L)\mu_{YZ}R \tag{48}$$

so that we have

$$Bw_B + Cw_C = -\{(1 + l_B + l_C)/L\}\mu_{YZ}R \tag{49}$$

The values of *l*'s are usually expected less than unity:

$$|l_B| \text{ and } |l_C| < 1 \tag{50}$$

and these conditions are satisfied in Table 1.

The signs of μ_{IY}, μ_{IIY}, and μ_{IIIY} given in eqs 43−45 and also the signs of Bw_B and Cw_C in eqs 47 and 48 are demonstrated in Figure 8. The results in Table 1 belonged to the d-zone, while those obtained previously in the hydrogenation reaction of propene belonged to a- and c-zones.[10,11]

5.5. Chemical Potentials of the Intermediates. The various results calculated from *l*'s according to eqs 39−49 are summarized in Tables 2 and 3. The results of chemical potentials are illustrated in Figure 9. Since the free energy decreased in the reaction sequence of CO(g) → CO(a) → CO_2(g) as shown in Figure 9a, it can proceed spontaneously, while the first and third steps in the reaction sequence of (1/2)O_2(g) → (1/2)O_2(a) → O(a) → CO_2(g) are against the reaction as shown in Figure 9b, although they are coupled.

The surface chemistry of Pt group metals in the presence of CO and O_2 is complex; the mechanism of CO oxidation may vary as a function of temperature, total pressure, ratio of the reactants, pretreatment of a polycrystalline sample, and crystal plane in single-crystal work.[1,2] Various kinds of CO−oxygen interaction on the surface have been studied. For instance, it is found that (i) active part of "O-rich" ruthenium phase is RuO_2, (ii) the RuO_2(110) surface exposes bridging oxygen atoms and ruthenium atoms not capped by oxygen, (iii) the latter act as coordinatively unsaturated sites onto which carbon monoxide can chemisorb and from where it can react with neighboring lattice-oxygen to carbon dioxide, and (iv) under steady-state conditions, the consumed lattice-oxygen is continuously restored by oxygen uptake from the gas phase.[16] The oxygen uptake process suggests correlation between the elementary reactions; process IIX, CO(a) → CO_2(g), may help process IY, O_2(g) → O_2(a).

Using a molecular beam technique, it is found that reactive scattering of CO molecules at oxygen-rich Ru(0001) surfaces at temperatures above 500 K is controlled by the diffusion of oxygen atoms from the near-surface region toward the surface.[17] The diffusion of subsurface oxygen is favorable to the result that the last stage IIIY, O(a) → CO_2(g), is against the reaction.

The free-energy dissipations in the reaction sequence of X ⇆ A → Z given by eq 41 was negative, whereas the net dissipation in the other sequence of Y ⇆ B ⇆ C → Z given by eq 49 was positive. The results suggest that CO(g) plays an active role in the overall reaction but O_2(g) plays a passive role.

5.6. Concluding Remarks. A central question of CO oxidation has been whether the reaction takes place between two adsorbed species (Langmuir−Hinshelwood mechanism) or between a gas-phase CO molecule and an oxygen adatom (Eley-Rideal mechanism).[2] The mechanism shown in Figure 6 evidently covers both mechanisms. Further, another elementary reaction of an adsorbate-induced surface reconstruction[18] formulated as

$$O_2(a) + CO(a) \rightarrow CO_2(g) + O(a) \tag{51}$$

could be considered by correlation between IIY and IIX or IIIY.

It should be emphasized that only if a definite reaction mechanism has been established, characteristic functions such as eqs 26−31 can be deduced analytically without any premises of (i) the law of mass action, (ii) use of uniform concentrations in rate expressions, (iii) adherence to particular isotherm models, and (iv) adherence to ideal catalytic surfaces. Though the present results leave room for more accurate investigation and for extensions to other experimental conditions, these results do point to the efficiency of this FR method.

6. Conclusions

The advantages of the present method are as follows: (i) Any rate equation can be linearized, because the perturbation is small, (ii) since the perturbation is harmonic, characteristic functions to explain FR data can be deduced analytically from a reaction mechanism adopted, (iii) a variety of rate coefficients involved in the characteristic functions can be determined owing to additional variable ω scanned over a wide range (similar to the frequency in a spectrum analysis), and (iv) since free-energy dissipations via intermediates can be deduced from the novel

rate coefficients, *l*'s, the FR method would be valid to detect the driving force in a catalytic reaction.

Acknowledgment. This work was partly supported by Grant-in-Aid for Scientific Research (C) (Grant 11640500) from the Ministry of Education, Culture, Sports, Science, and Technology, Japan.

References and Notes

(1) Engel, T.; Ertl, G. *Adv. Catal*. **1979**, *28*, 1.
(2) Engel, T.; Ertl, G. *The Chemical Physics of Solid Surfaces and Heterogeneous Catalysis, Vol. 4;* King, D. A., Woodruff, D. P., Eds.*;* Elsevier: Amsterdam, 1982; Chapter 3.
(3) Imbihl, R.; Ertl, G. *Chem. Rev*. **1995**, *95*, 697.
(4) Oertzen, A. v.; Rotermund, H. H.; Mikhailov, A. S.; Ertl, G. *J. Phys. Chem. B* **2000**, *104*, 3155.
(5) Weller, S. W. *Catal. Rev.—Sci. Eng*. **1992**, *34*, 227.
(6) Bennett, C. O. *Adv. Catal*. **1999**, *44*, 329.
(7) Gravers, M.; Davidson, J. M.; Harkness, I. R.; McDougall, G. S.; Rees, L. V. C. *Stud. Surf. Sci. Catal*. **1999**, *122*, 65.
(8) Yasuda, Y. *Heterogen. Chem. Rev.* **1994**, *1*, 103.
(9) Yasuda Y. *J. Phys. Chem*. **1989**, *93*, 7185.
(10) Yasuda, Y. *J. Phys. Chem. A* **1998**, *102*, 7185.
(11) Yasuda, Y.; Kuno, Y. *J. Phys. Chem. B* **1999**, *103*, 3916.
(12) Boudart, M.; Tamaru, K. *Catal. Lett.* **1991**, *9*, 15.
(13) Yasuda, Y.; Iwai, K.; Takakura, K. *J. Phys. Chem.* **1995**, *99*, 17852.
(14) Moula, M. G.; Wako, S.; Cao, G.; Kimura, K.; Ohno, Y.; Kobal, I.; Matsusima, T. *Phys. Chem. Chem. Phys*. **1999**, *1*, 3677.
(15) Because w_A is an intensive property, w_A should not depend on ΔP's or ΔV.
(16) Over, H.; Kim, Y. D.; Seitsonen, A. P.; Wendt, S.; Lundgren, E.; Schmid, M.; Varga, P.; Morgante, A.; Ertl, G. *Science* **2000**, *287*, 1474.
(17) Boettcher, A.; Rogozia, M.; Niehus, H.; Over, H.; Ertl, G. *J. Phys. Chem. B* **1999**, *103*, 6267.
(18) Dicke, J.; Rotermund, H. H.; Lauterbach, J. *Surf. Sci.* **2000**, *454—456*, 352.